Energy straggling of protons in Be, C, Al, and Si

R. A. Langley* and D. K. Brice
Sandia Laboratories, Albuquerque, New Mexico 87185
(Received 8 May 1978)

Ion backscattering from solid targets of elements with prominent structure in their (p,p) scattering cross section has been used to measure the energy straggling of protons in Be, C, Al, and Si. Single-crystal targets were used in order to minimize porosity, channeling, and surface-roughness effects. In order to obtain straggling parameters from the experimental data, corrections for contributions, other than those mentioned above, to the broadening of the observed spectra were made. The energy dependence of the stopping power of the target for the protons makes a significant contribution to the broadening of the observed backscattering spectra, and must be properly accounted for if precise values of the straggling parameters are to be obtained. A procedure is described for accomplishing this. Using the experimental technique and analysis procedure described, proton straggling was evaluated in Be, C, Al, and Si in the energy range 100–3000 keV. The results are summarized by defining $f \equiv \Omega/\Omega_B$, where Ω_B is the straggling predicted by the Bohr theory. The results are:

Be ($E_{res}=2.530$ MeV), $f=1.0^{+0.3}_{-1.0}$
C ($E_{res}=0.47$ MeV), $f=0.0^{+1.5}_{-0.0}$
C ($E_{res}=1.73$ MeV), $f=0.9\pm0.1$
Al ($E_{res}=2.480$ MeV), $f=1.25\pm0.2$
Al ($E_{res}=2.555$ MeV), $f=1.25\pm0.2$
Si ($E_{res}=1.682$ MeV), $f=1.15\pm0.2$
Si ($E_{res}=2.099$ MeV), $f=1.4\pm0.3$

In addition to the straggling results, relative elastic scattering cross sections were determined for protons on Be (2.25–2.85 MeV, $\theta_{lab}=170°$) and on Al (2.4–2.6 MeV, $\theta_{lab}=170°$).

I. INTRODUCTION

Although extensive studies of the distribution of energy losses (energy straggling) of beams of particles traversing solids have been carried out in the past, until recently, relatively little attention has been given to the velocity regime corresponding to protons or α particles with energies below a few MeV. The use of atomic beams as probes of the near surface region of solids has, however, stimulated renewed interest in straggling at these low energies, since this is one of the principal factors limiting the depth resolution of such experiments. Thus, it is important to understand and quantitatively measure straggling for such practical applications. Recent refinements in the theory[1–5] of straggling for low incident energies are a further incentive for carrying out such measurements. This energy region has probably not received broad attention in the past because straggling is in general a second-order effect, and it is difficult to measure accurately.

A variety of phenomena contribute to the broadening of the energy spectrum as the incident projectiles lose energy in the target material. In addition to the distribution of fundamental energy losses, these phenomena include, for example, target inhomogenities such as porosity,[6] nonuniform film thickness,[7,8] surface roughness,[9] etc. In addition, channeling effects in crystalline or polycrystalline targets are thought to contribute to the broadening observed in such experiments.[9] In order to be able to understand the basic properties of the target material, it is thus important to eliminate or independently measure as many of these individual contributions as possible.

Most of the phenomena which contribute to the broadening are statistically independent of one another and, under these conditions, the total straggling is simply the sum, in quadrature, of the various individual contributions. The separation of the various contributions in this case is thus mathematically straightforward. Among those effects which meet the criterion of statistical independence are those mentioned in the previous paragraph as well as instrumental effects such as spread in the incident beam energy, and detector resolution.

Another phenomenon which contributes to the observed broadening, and which is not independent of the other broadening processes, is the energy dependence of the target stopping power $S(E)$ for the incident projectiles. The origin of the stopping-power

effect (SPE), and its dependence on the other broadening processes, is readily explained by reference to Fig. 1. Figure 1 shows, schematically, the distribution in energy of a beam of projectiles at two different depths in a target material. Because of the energy dependence of $S(E)$ the two groups of projectiles labeled A and B in the shallower of the two distributions will have different energy-loss rates. Thus, because of the different loss rates additional penetration of the target to the depth of the second distribution will lead to a change in the energy separation ΔE between the groups A and B, thereby changing the width of the distribution. If $S(E)$ is a decreasing function of E, the distribution will be broadened (high-energy case), while if $S(E)$ is an increasing function of E, the distribution will be narrowed (low-energy case).[10] It is also clear from Fig. 1 that the SPE is dependent on prior broadening by other processes, since this effect of differing energy-loss rates requires projectiles with different energies.

Since the straggling of a beam of particles traversing a target material can significantly affect the observed width of sharp features (e.g., elastic scattering resonances, edges due to interfaces, etc.) which are present in backscattering spectra, these features can be used to accurately measure the energy straggling. The technique has previously been described by Olmos *et al.*,[9] who used elastic scattering resonances to measure the energy straggling of 0.5–5-MeV protons in carbon. Their results indicate that the straggling is 4–5 times that predicted by the basic Bohr theory,[11] results which seem inexplicable even with the more recent refinements to the theory.[1–5] They did not include a consideration of the SPE in the analysis of their data, however, and we believe that this can account for the major portion of the discrepancy between their results and the theoretical predictions.

In this work we have repeated the measurements of Ref. 9, using essentially the same experimental technique. We have attempted, however, to eliminate surface roughness and channeling effects from our measurements, since they were thought to contribute to the uncertainty in the earlier results. We have also developed an analytical procedure which allows us to include the effects of the SPE in extracting the straggling from the experimental data, and which illustrates the importance of SPE in such experiments. Also, in order to further investigate the advantages and limitations of this technique for such measurements, we have determined the energy straggling for protons with energies below 3 MeV in Be, Al, and Si.

We present a discussion of the experimental method in Sec. II, a discussion of the method of data analysis in Sec. III, and finally new results for the straggling of protons in beryllium, carbon, aluminum, and silicon in Sec. IV.[12]

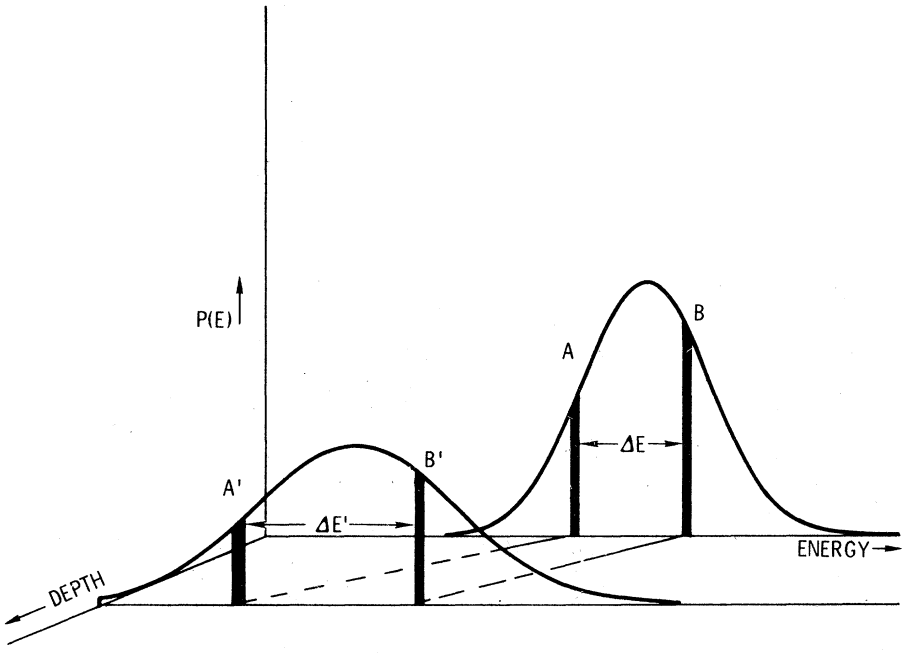

FIG. 1. Schematic illustration of the physical processes underlying the stopping-power effect. $P(E)$ represents the distribution in energy E of the incident projectiles after some penetration of the target material. Particles in the two groups labeled A and B are separated in energy by ΔE in the shallower distribution. After an additional penetration into the target the energy separation of the two groups changes to $\Delta E'$ due to the energy dependence of $S(E)$.

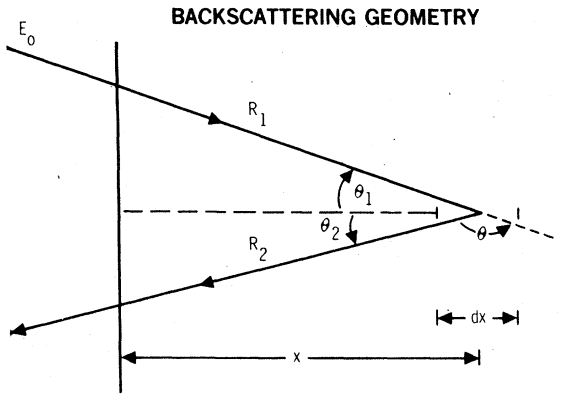

FIG. 2. Typical geometry of a backscattering experiment showing the relationships between depth x, inbound path length R_1, outbound pathlength R_2, and the incident and emergent angles θ_1 and θ_2, respectively. Also shown is the scattering angle θ.

II. EXPERIMENTAL METHOD

Many previous measurements of energy straggling have relied on the thickness uniformity of deposited films.[7,8] Since the observable effects which result from thickness nonuniformity and straggling are the same, it is necessary to independently measure the thickness uniformity in order to accurately determine the straggling. Although such measurements can often be made, the lateral resolution is usually quite poor. However, for materials containing elements having prominent features in their scattering cross section, energy straggling can be accurately measured without reliance on the thickness uniformity of thin films. The procedure consists of bombarding a bulk sample with monoenergetic ions and measuring the energy spectrum of the backscattering particles for incident energies above the resonance energy. Figure 2 shows the geometrical arrangement and defines the parameters involved. As the incident energy E_0 is increased above the resonance energy, the resonance occurs deeper in the material. The straggling of particles scattered at the resonance is thus increased, thereby increasing the observed resonance width. This is illustrated in Fig. 3 for the 1.73-MeV elastic scattering resonance $^{12}C(p,p)^{12}C$. Using the measured increase in width the straggling can accurately be extracted from such measurements if other broadening effects have been eliminated or are properly accounted for, e.g., channeling, porosity, surface roughness, and stopping power effects. The resonances used in the measurements and pertinent information on experimental arrangements is given in Table I.

The accuracy with which the straggling parameter Ω can be determined is dependent on sharpness of the

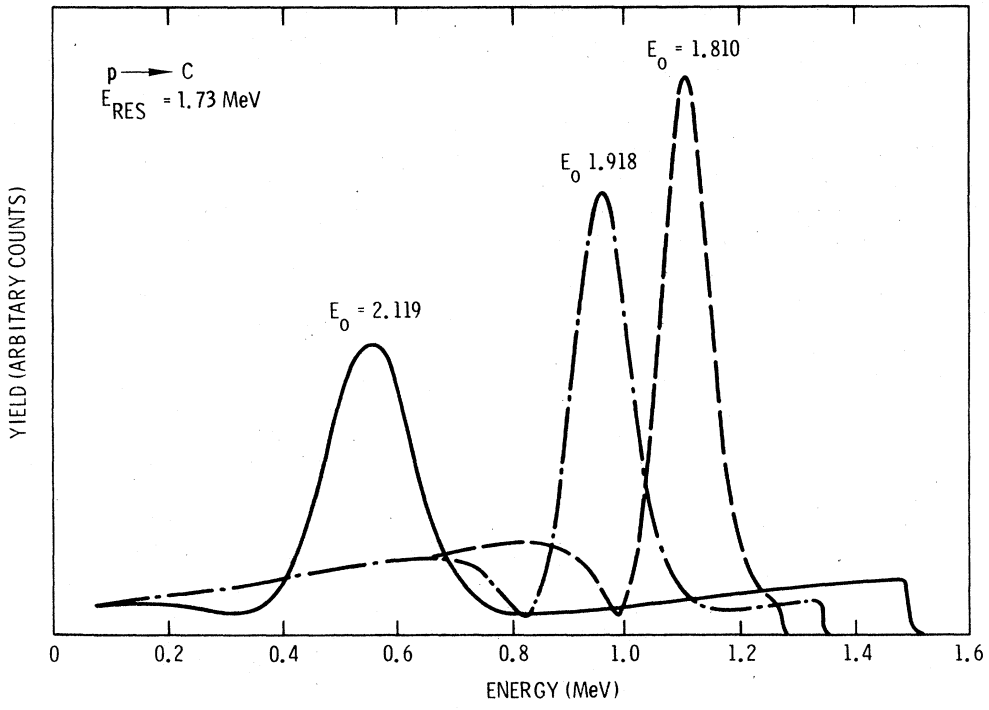

FIG. 3. Backscattering spectra for protons in carbon for various incident energies; E_0 (MeV) = 1.810, 1.918, and 2.119. The prominent feature is the 1.73-MeV elastic scattering resonance.

TABLE I. Resonances and crystallographic orientations used in the experimental measurements.

Resonance	Resonance energy (MeV)	Orientation of incident beam to crystal axes	Elastic cross-section reference
$^{9}Be(p,p)$	2.530	15° off ⟨0001⟩ (⟨0001⟩ normal to surface)	13
$^{12}C(p,p)$	0.470 1.730	20° off ⟨0001⟩ 30° off $\{1\bar{1}00\}$ 30° off $\{01\bar{1}0\}$ (⟨0001⟩ normal to surface)	14,15
$^{27}Al(p,p)$	2.480 2.555	12° off ⟨001⟩ 15° off {110} 30° off {100} (⟨001⟩ normal to surface)	16–18
$^{28}Si(p,p)$	1.682 2.099	15° off ⟨100⟩ 15° off {100} 30° off {110} (⟨100⟩ normal to surface)	19

resonance. If the resonance is broad, which is the case for the 2530-keV ^{9}Be and the 470-keV ^{12}C resonances, only upper limits can be determined for Ω.

A single crystal of Be was prepared by the Franklin Institute, starting with polycrystalline material which had as principal metallic impurities Fe(165 ppm by weight), Ni(105 ppm), Si(82 ppm), Ar(60 ppm), Mg(44 ppm), and Cu(40 ppm), with others totaling less than 50 ppm. Beryllium oxide was present in much larger quantities, about 9000 ppm by weight. Three zone passes were used to lower the level of metallic impurities, which backscattering analysis showed to be reduced by about a factor of 2 below that given for the polycrystalline material. After being planed the samples were electropolished to remove the cutting damage. The orientation of samples was confirmed by x-ray diffraction. The mosaic spread of one sample was also measured during x-ray diffraction, and found to be 0.6° full width at half-maximum (FWHM). This mosaic spread was large enough to preclude measurements of a channeling dip. The crystal was positioned so that the incident beam was 15° off the c axis.

The carbon material chosen for this study was compression annealed pyrolytic graphite (CAPG). It is a material whose structure closely approximates that of a single crystal.[20] New flat surfaces were prepared before the experiment by peeling off many atomic layers. The sample was first studied by axial channeling to determine the orientation of the c axis and the "quality" of the crystal. The FWHM of the channeling dip obtained experimentally was equal to the calculated value for a perfect crystal within the experimental error.

Single crystals of aluminum and silicon were used. Alignment of the ⟨001⟩ and ⟨100⟩ axes with the surface normal was checked with x-ray diffraction for Al and Si, respectively. The samples were studied by axial channeling to determine the orientation of these axes and the "quality" of the crystals. For both crystals the FWHM of the channeling dip obtained experimentally was equal to the calculated value for a perfect crystal within experimental error.

For all four materials the detected beam was 170° from the incident beam and 10° further from the major axis than the incident beam so that the alignment should have produced a geometry in which both the incident beam and the detected scattered beam were removed from any major axial or planar direction, thus reducing channeling effects to a minimum. By using perfect and near perfect crystals, both porosity and surface roughness effects were minimized.

The experiment was carried out using an accelerator and associated equipment, which has been fully described elsewhere.[21] Only the more pertinent points will be reviewed. The accelerator nominal highest voltage 2.5 MeV, and analyzing magnet combination provides a beam of nearly monoenergetic protons(± 1 keV) of variable energy and directs the beam onto the target. The absolute energy of the beam was determined to within 8 keV by using a radioactive ^{241}Am source[22] and the $^{19}F(p,\alpha\gamma)$ resonance.[23] The angular

divergence of the incident beam at the target was less than 0.02°. The target chamber is described in Ref. 21 and the target manipulator in Ref. 24. A gold barrier silicon detector was used to detect the scattered particles and was placed so that it intercepted a portion of the beam scattered about 170°. The solid angle subtended by the detector was 0.01 sr. The energy resolution of the detector-analyzer system was approximately 10 keV.

The data were collected by initially using an incident beam energy slightly greater than the resonance energy (~30 keV) and increasing this energy in successive steps until the particles scattered at the resonance energy had energies below ~200 keV after leaving the target surface. Typical backscattering spectra are shown in Figs. 3 and 4 for the 1730-keV and 475-keV $^{12}C(p,p)$ resonance, respectively. the lower-energy resonance is broad while the upper resonance is sharp. The effect of the resonance width is reflected in the shapes of the spectra.

III. DATA ANALYSIS

A. Theory

In this section a procedure will be described which allows the energy straggling to be extracted from the experimental data. Since the broadening of the observed resonances by the SPE is not independent of the energy straggling this procedure is somewhat complex, but nevertheless tractable.

Strictly speaking, the SPE should not be considered as a contribution to the measured straggling, although it does contribute to the observed broadening. Straggling is due to a *statistical* distribution of the energy losses, and as such implies a loss of information. Thus, for example, the depth resolution in backscattering analysis becomes poorer as the beam penetrates deeper into the target material because of the loss of information due to straggling. In the absence of a statistical distribution of energy losses, however, the depth distribution in such experiments is limited only by the initial width of the resonance being observed and by instrumental properties. In this case, although the SPE is operative in changing the observed width of the feature in the backscattering spectrum, no information is lost, and apart from the instrumental effects just mentioned, the depth resolution would be independent of depth in the target material. In the same fashion, the narrowing of the distribution by the SPE at low energies does not imply a gain in information.

The significance of the SPE for an initially monoenergetic beam of particles *transmitted* through a thin target has previously been investigated by Tschalär.[25] He finds that the stopping-power effect is negligible compared to the other broadening processes for total energy loss 20%–30% of the initial kinetic energy of the projectile. This results because in transmission the

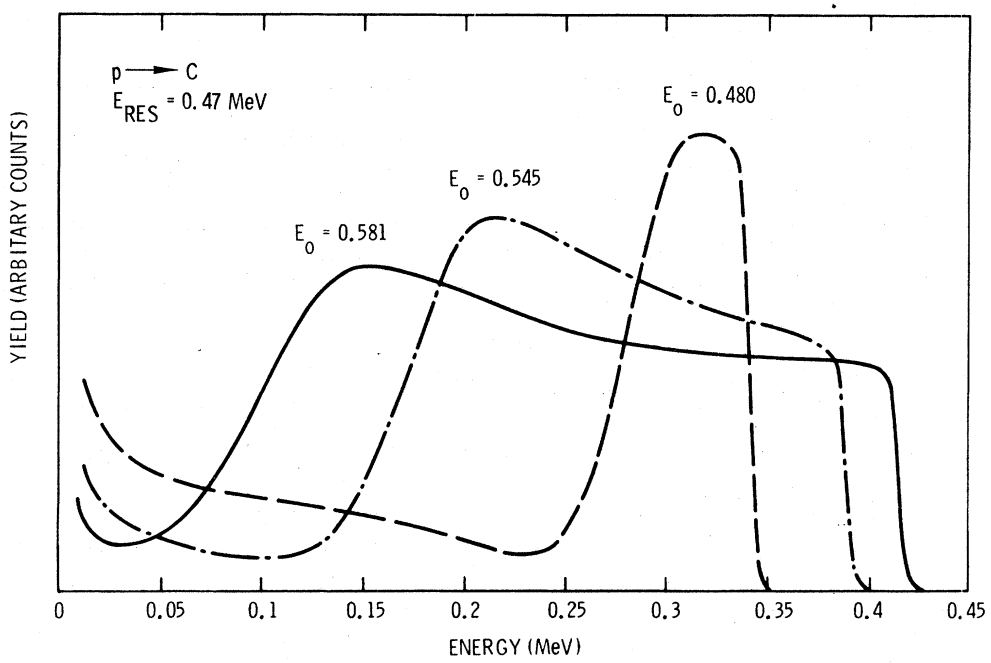

FIG. 4. Backscattering spectra for protons in carbon for various incident energies; E_0 (MeV) = 0.480, 0.545, and 0.581. The prominent feature is the elastic scattering "edge" at 0.470 MeV.

broadening by other processes is sufficiently small that no appreciable spreading of the projectile energy distribution occurs until the projectiles have penetrated deep into the target material. In the *backscattering* case, however, significant broadening of the projectile energy distribution can be realized at relatively shallow depths due to the backscattering event itself, e.g., due to the natural width of a scattering resonance.

The significance of SPE in the backscattering case can be demonstrated by direct calculation of spectra from the standard backscattering equation[26] which gives the yield in the absence of energy straggling and instrumental broadening processes. In Table II the FWHM of calculated spectra for scattering from the 1.73-MeV(p,p) resonance in carbon is given for several incident proton energies. Also tabulated is the FWHM from the present experimental measurements and the calculated depth at which the incident proton energy is reduced to 1.73 MeV. The calculations used experimental scattering cross sections and stopping-power values. For constant $S(E)$ the calculated FWHM is 85 keV, independent of the incident energy. The tabulated data indicate that as the incident energy is increased from 1.8 to 2.1 MeV, the observed resonance width increases from 102 to 186 keV. The calculated FWHM shows that much of this broadening is due to SPE.

Since the action of the SPE in broadening the observed energy distributions is dependent on prior broadening by other processes it is not possible to account for all broadening by simply adding the individual contributions in quadrature. The determination of the total broadening of the observed spectra thus requires a proper mathematical description. A simple approximate formula for the total effect of the various broadening processes has previously been derived by Deconninck and Fouilhe, but its applicability seems restricted to relatively narrow symmetric scattering resonances which are well separated from other features in the spectrum.[27] We now present a procedure for the precise calculation of the observed spectrum in the general case, which allows the various contributions to be separated.

For the geometry of Fig. 2 the backscattered yield $Y(E',\theta)\,dE'$ from a distribution of scattering centers $N_s(x)$, at a depth x within the target material is given by

$$Y(E',\theta)=\frac{\Phi}{\cos\theta_1}\int_0^\infty N_s(x)\,dx\int_0^\infty P_1(E,E_0,R_1)\times P_2(E',KE,R_2)\,\sigma(E,\theta)\,dE \quad . \tag{1}$$

Here $P_1(E,E_0,R_1)$ is the distribution in energy E of the incident ions after they have penetrated a distance $R_1(x)$ along the inbound trajectory, including any spread in the incident energy E_0. Similarly, $P_2(E',KE,R_2)$ is the distribution in energy E' of ions emerging from the target surface after they were backscattered at energy E and depth x within the target. Any spread in observed energies E' due to detector resolution is included in P_2. The backscattering factor K relates the scattered energy to the energy just before scattering. The differential atomic scattering cross section for this event is $\sigma(E,\theta)$; the incident angle θ_1, emergent angle θ_2, and scattering angle θ, are related as indicated in Fig. 2; the incident ion fluence is Φ. Path length straggling due to multiple scattering is implicitly included in the general equation (1), but the effect of angular dispersion is not. The latter effect is generally quite small for typical large-angle backscattering arrangements.

Since each of the individual distributions P_1 and P_2 is formally a transmitted distribution (in the sense of Tschalär[25]), the broadening of P_1 and P_2 by the SPE can normally be neglected compared with their broadening by other processes. The major contribution of the SPE to the broadening of the observed spectrum is thus due to groups of ions coming from different regions of the scattering resonance. That is, the action of the SPE *within* a group of nearly monoenergetic ions (e.g., groups A or B in Fig. 1) is quite small compared with its effect between groups with significantly different energies. Energy straggling and instrumental effects are then the only significant

TABLE II. Stopping-power effect for protons scattered through 170 by the elastic-scattering resonance at 1.73 MeV in carbon.

Incident energy E (keV)	Penetration depth for $E_p=1.73$ MeV (10^{19} C/cm^2)	Observed Resonance Width FWHM (keV) Calculation (SPE only)	Experiment (SPE plus straggling)
1800	2.6	104.1	102.4 ± 2.0
1900	6.2	116.9	119.2 ± 2.0
2000	9.8	134.8	140.3 ± 2.0
2100	13.4	172.0	185.5 ± 2.0

broadening processes acting on P_1 and P_2. In most cases Gaussian functions are thus adequate for both P_1 and P_2. In this case

$$P_k(E,E_i,R_k) = (2\pi\Delta_k^2)^{-1/2} e^{-(E-E_a)^2/2\Delta_k^2} , \tag{2}$$

where

$$\Delta_k^2 = \Delta_{0k}^2 + \Omega^2(R_k) . \tag{3}$$

In (3) the quantity Δ_{0k} represents the spread in incident beam energies for $k=1$, the detector resolution for $k=2$. Energy straggling of the beam is represented by $\Omega^2(R_k)$. In the absence of multiple-scattering effects the average energy in the distribution E_a is related to the initial energy E_i and the path length traveled R_k by

$$R_k(x) = \frac{x}{\cos\theta_k} = \int_{E_a}^{E_i} \frac{dE}{S(E)} . \tag{4}$$

To include path-length straggling due to multiple scattering the right-hand side of (4) is replaced by the projected range $R_p(E_i,E_a)$; further, $[S(E_a)\Delta R_p]^2$, where ΔR_p is the standard deviation in R_p,[28] is added to the right-hand side of (3). Multiple-scattering effects are small except for large energy losses, and they have been neglected in the present applications of (1).

Energy straggling parameters are extracted from experimental spectra by comparison with the spectra calculated with Eq. (1). The straggling parameters $\Omega^2(R_k)$ in the calculated spectra are varied to obtain a best fit between experiment and theory.

B. Application to experimental data

Although the application of the above procedure to the analysis of experimental data is straightforward in principle, in practice it is somewhat complicated. The analysis requires accurate values of the scattering cross section $\sigma(E,\theta)$, and the stopping power $S(E)$, and these quantities may be either not available in the literature, or not sufficiently accurate when they are. It should be pointed out that accuracy in the slope of S is the prime consideration in the present case (at least to first order) since the SPE is determined by the *difference* in energy-loss rates across the projectile energy distribution. S and/or σ were not available with sufficient accuracy for several of the targets considered here, and thus these functions were determined simultaneously with Ω^2 from the present experimental measurements. This was accomplished by an iterative procedure which is described briefly below.

The procedure begins by assuming trial functions for either or both of σ and S, and by using the standard Bohr prediction[10] for Ω^2. For this purpose a three-parameter description of S was used which is discussed elsewhere.[29] A theoretical spectrum is then calculated using Eqs. (1) and (4) and compared with an experimental spectrum for a case in which the incident proton energy is just slightly above the resonance energy. The theoretical spectrum is multiplied by a constant to give a minimum least-square deviation between the two spectra. The ratio of the two spectra is then taken, channel by channel, as a multiplicative correction to the trial function σ. This procedure is then iterated until the experimental and theoretical spectra converge.

Comparison of a theoretical and an experimental spectrum is next carried out in a similar fashion for a significantly higher incident proton energy. This time the parameter n in the three parameter description[29] of S is varied to bring the *locations* of the resonances in the two spectra into coincidence. The other two parameters are also varied simultaneously so that with n as chosen above the resultant function S also has a minimum deviation from tabulated stopping power values.[30] For the energy region of the present experiments, the parameter n principally determines the average slope of S, while the other two (along with n) determine magnitude as well as local curvature. With the new representation for S the procedure returns to the previous spectra and a new determination for σ is made. This process is iterated until both σ and S converge. Generally, one iteration has proven sufficient in all cases.

After the above determinations of representations for σ and S, the straggling parameter Ω^2 is extracted from spectra at several different incident proton energies. Since the values for Ω^2 which result from the analysis given here will be averages over inbound and outbound proton trajectories in the target material, it is not possible to obtain an accurate and detailed energy dependence of Ω^2, and so in the analysis it is assumed that Ω is a constant fraction f of the value predicted by Bohr theory.[10] This is

$$\Omega(R) = f\,\Omega_B(R) , \tag{5}$$

with

$$\Omega_B(R) = 4\pi N Z_1^2 Z_2 e^4 R , \tag{6}$$

where Z_1 and Z_2 are projectile and target atom atomic numbers, respectively, N is the target atomic density, R is the length of the projectile trajectory in the target, and e is the electronic charge. Calculated and measured spectra are compared as a function of f. The procedure is illustrated in Fig. 5 for the 1.73-MeV $^{12}C(p,p)^{12}C$ resonance.

For a particular value of f the magnitude of the calculated spectrum is adjusted to give the least mean-square error δ^2 between experiment and theory. The quantity δ is determined as a function of f to obtain that value of f which gives the best overall fit (i.e.,

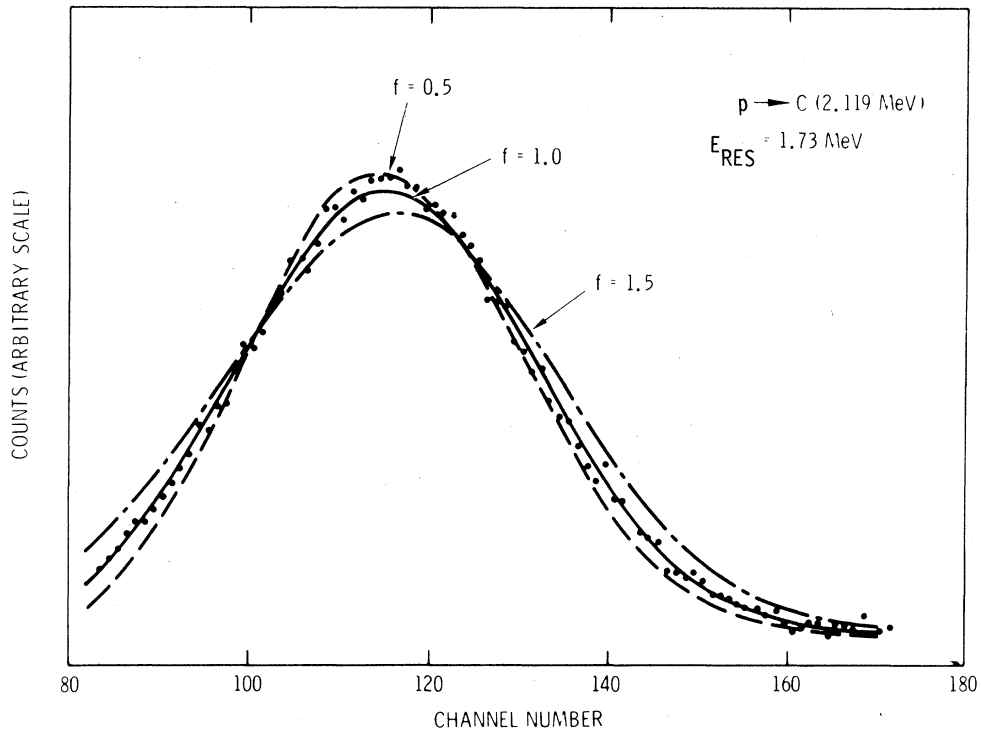

FIG. 5. Comparison of experimental backscattering spectrum for scattering of protons from the 1.73-MeV(p,p) resonance in carbon with calculated spectra for which the energy-straggling parameter Ω has been varied.

minimum δ) between the calculated and measured spectra. In this way an accurate determination of Ω^2 is obtained. Once Ω^2 has been determined by such a procedure the whole process is repeated from the beginning and iterated until representations for S, σ, and Ω^2 are obtained which are consistent with all the experimental data.

IV. RESULTS

The δ vs f curves obtained in the analysis described above for protons incident on Be and C targets are presented below. The uncertainties assigned to the f values at the curve minima were estimated through the use of two criteria. One estimate was obtained through the fluctuation expected in δ due to counting statistics. The standard deviation in such fluctuations for the present measurements can easily be shown to be $\sim$10%–15% of $N_{\text{exp}}^{1/2}$, where N_{exp} is the total number of counts in a given spectrum. The second estimate used the position on either side of the minimum at which the δ vs f curves become essentially linear. The uncertainties in f which result from these estimates normally range from 10% to 20%, although for Be and one resonance in C the uncertainties are much larger.

A. Beryllium

Backscattering spectra were obtained fror a number of different incident proton energies in order to carry out the analysis described in Sec. III. The analysis was ultimately performed using spectra for incident proton energies of 2.604 and 3.006 MeV. Since cross-section data could not be found in the literature for scattering at 170° in laboratory coordinates, it was necessary to determine this quantity during the analysis. Figure 6 shows the relative elastic scattering cross section so obtained for proton energies between 2.25 and 2.85 MeV. Cross-section data for this resonance has previously been reported[13] for center of mass scattering at angles up to 160°. The resonance at 170° is narrower than that observed at the smaller angles, as is typical in such measurements.

The stopping power was also obtained in the analysis. The values obtained for the parameters Z, a, n for the stopping power formula[29] are given in Table III. The rms deviation between the S values given by the formula and those tabulated by Janni[30] is less than 5% over the energy range 0.2–0.3 MeV.

The rms deviation δ between the calculated and measured spectra for an incident proton energy of 3.006 MeV is shown in Fig. 7 as a function of f. The

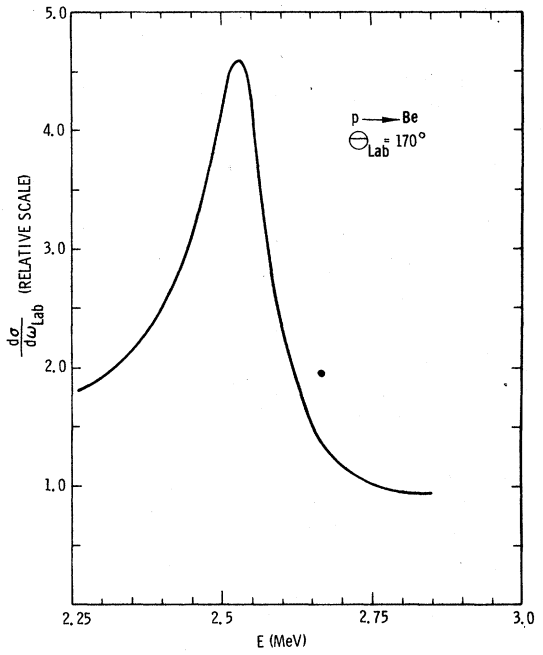

FIG. 6. Relative elastic scattering cross section at 170° in laboratory coordinates for 2.25–2.85-MeV protons incident on Be.

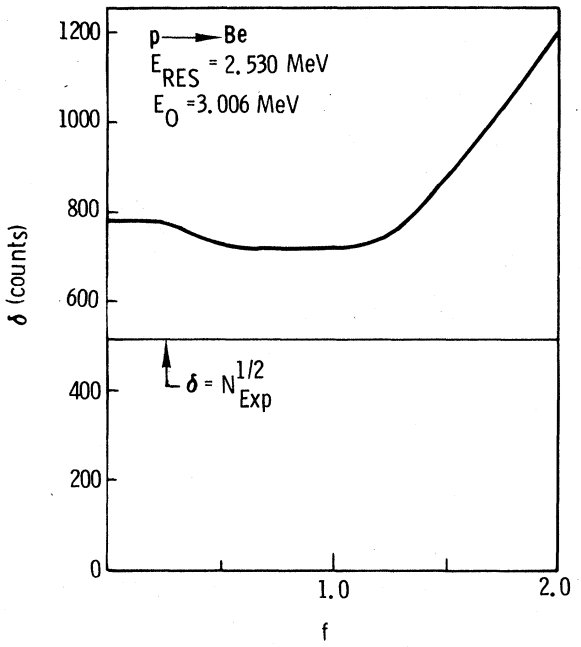

FIG. 7. Plot of rms deviation between calculated and experimental backscattering spectra δ as a function of f $(=\Omega/\Omega_B)$, for the 2.530-MeV elastic scattering resonance in Be. N_{exp} is the number of counts in the experimental spectrum.

horizontal line at $N^{1/2}_{exp}$ represents essentially the best agreement which could be expected between the calculated and experimental spectra. From Fig. 7 is is seen that the best value of f (i.e., minimum δ) is $f = 1.0^{+0.3}_{-1.0}$. The large uncertainty in f, and the relatively large disparity between the minimum value of δ and $N^{1/2}_{exp}$ results from the relatively large width of the scattering resonance and suggests one of the limitations of this type of measurement. The value obtained for f is of course its average value over the energies experienced by the protons on their inbound and outbound trajectories which span the energy ranges 2.45–3.0 and 0.2–1.7 MeV, respectively.

TABLE III. Stopping power formula parameters Z, a, n for protons on Be, C, Al, and Si.

Target	Z	a	n
Be	2.481	0.3886	3.543
C	1.394	0.5684	3.388
Al	2.910	0.4133	3.252
Si	2.533	0.4650	3.188

B. Carbon

The elastic scattering cross section for proton scattering from carbon is available in the literature,[14,15] and two resonances were utilized in our analysis of this material. The resonances are located at 1.73 and 0.47 MeV. The stopping power formula parameters used for the analysis are given in Table III. The formula values for $S(E)$ using these parameters differ from the values tabulated by Janni[30] by less than 2% over the energy range 0.1–3.0 MeV.

The curve of δ vs f is shown in Fig. 8 for the 1.73 MeV resonance. The experimental spectrum used in this analysis was obtained with an incident energy of 2.119 MeV. The energies experienced by the protons on the inbound and outbound trajectories spanned the ranges 1.70–2.12 and 0.40–1.22 MeV, respectively. From Fig. 8 it is seen that the best value of f is 0.9 ± 0.1.

The curve of δ vs f for the 0.47-MeV resonance is shown in Fig. 9. The incident energy was 0.585 MeV for this case, and the inbound and outbound trajectories spanned the energy ranges 0.430–0.585 and 0.025–0.310 MeV, respectively. The best value of f for this case is $0.0^{+1.5}_{-0.0}$. The large uncertainty in f

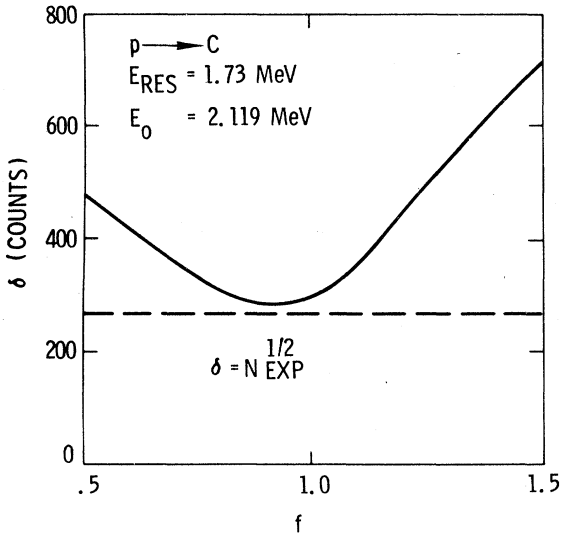

FIG. 8. Plot of δ vs f for elastic scattering of protons from the 1.73-MeV elastic scattering resonance in C. N_{exp} is the total number of experimental counts.

results from the relatively large width of the resonance as well as the relatively shallow depth of penetration which could be attained by the protons.

C. Aluminum

The elastic scattering cross section for protons on aluminum was not available for scattering at 170° in laboratory coordinates.[16–18] The relative cross section was therefore determined by our analysis using spectra obtained at incident energies of 2.587, 2.625, and 3.001 MeV. The relative cross section which resulted is shown in Fig. 10 for proton energies in the range 2.42–2.62 MeV. The two large resonances at 2.480 and 2.555 MeV were used concurrently in the analysis to determine the best representation for $S(E)$ and a value for f. It was not possible to obtain a representation for $S(E)$ which resulted in coincidence between calculated and measured location in the spectra of both resonance peaks simultaneously. The origin of this difficulty is not understood. The analysis was carried out with several different representaions to determine the effect of uncertainties in $S(E)$ on the resultant values obtained for f. Fortunately, the resonances are relatively narrow and the small uncertainty in the slope of $S(E)$ had no significant effect on the best f value extracted from the analysis. The stopping power formula parameters given in Table III for the aluminum targets represent a compromise among the various representations used.

The best value of f is found to be 1.25 ± 0.2. The energy ranges over which this f value has been averaged are 2.45–3.00 and 1.20–2.10 MeV for the inbound and outbound trajectories, respectively.

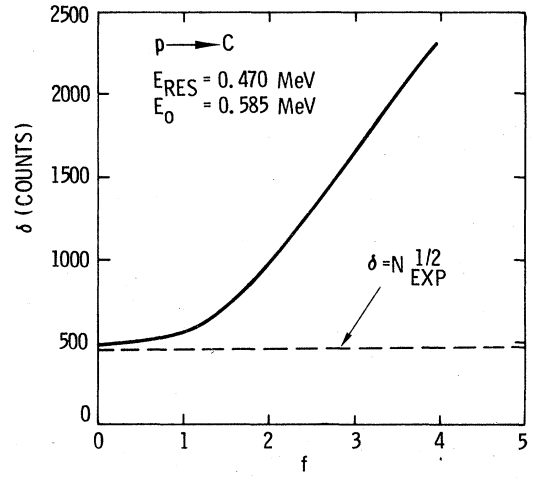

FIG. 9. Plot of δ vs f for elastic scattering of protons from the 0.47-MeV elastic scattering resonance in C. N_{exp} is the total number of experimental counts.

D. Silicon

The elastic scattering cross section for the silicon analysis was obtained from Ref. 19. Spectra used in the analysis were taken with incident proton energies of 2.210, 2.843, and 2.933 MeV. The scattering resonances at proton energies of 1.682 and 2.099 MeV were used to obtain f values. The stopping power formula parameters used in the analysis are given in Table III.

For the 2.099-MeV resonance the best value for f is 1.4 ± 0.3. This f value is an average over the energy ranges 2.07–2.93 and 0.27–1.79 MeV for the inbound and outbound trajectories, respectively. For the

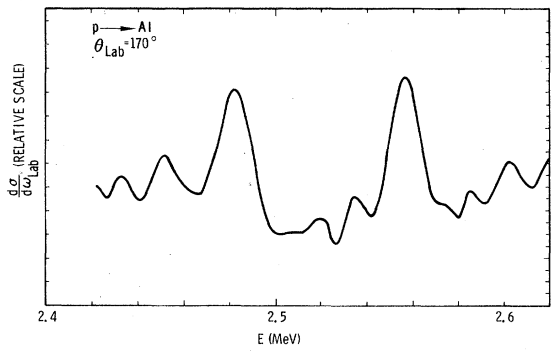

FIG. 10. Relative elastic scattering cross section at 170° in laboratory coordinates for 2.42–2.62-MeV protons incident on Al.

1.682-MeV resonance the best value for f is 1.15 ± 0.2. The energy ranges over which this f value has been averaged are 1.60–2.21 and 0.40–1.39 MeV for the inbound and outbound trajectories, respectively.

E. Discussion

Direct comparison of the results of the present measurements of proton energy straggling (summarized in Table IV) with previous experimental measurements can be made in only a few cases because of the sparsity of such data in the literature. Early measurements for Be targets[31] and Al targets[31,32] show considerable scatter, but in general are in agreement with the present measurements. More recent measurements for 0.1–0.5-MeV protons on Al targets[33] indicate that f should be an increasing function of energy varying from 0.9 to 1.1 in this energy range. Although the energy range investigated in the present case is somewhat above 0.5 MeV, the general trend of the measurements in Ref. 33 suggests that a value of f greater than one is to be expected.

Theoretical calculations of the energy dependence of proton energy straggling have been carried out by Bonderup and Hvelplund[1] using a statistical model of the target atom charge distribution, and by Chu[2] using a Hartree-Fock-Slater charge distribution for the target atoms. Both these calculations are based on an extension of the Lindhard-Sharff procedure,[34] in which the local charge density in the target atom is considered to respond as a free-electron gas. All these theories[1,2,34] predict that for the energy range of the present experiments the f values should lie between 0.8 and 1.0, for fixed proton energy the f values should be a decreasing function of target atomic number Z_2, and for a fixed Z_2 the f values should be an increasing function of the proton energy. The results in Table IV for both C and Si targets suggest that f *is* an increasing function of proton energy, although this trend does not lie outside the uncertainty of the measurements. Comparison of the results for C, Al, and Si indicates, however, that the expected Z_2 dependence is not obeyed in the present measurements. Further, the magnitudes of the f values for Al and Si are clearly greater than predicted. These discrepancies between the theoretical work and the present experimental measurements suggest that significant contributions to the proton straggling are produced by phenomena which have been neglected in these theories.[1,2,34] Such phenomena include, for example, energy-loss fluctuations due to charge changing collisions[4,5] (which were invoked by Bednyakov *et al.*,[33] to explain their relatively large f values for Al targets), as well as correlation effects in energy loss along the projectile trajectory which have been shown by Sigmund[3] to increase the measured straggling by as much as 35% in molecular gas targets (thus increasing the f value by 17%).

TABLE IV. Average values of f obtained in the analyses over the indicated energy ranges.

Target	Average f value	Energy range averaged over (MeV)
Be	$1.0^{+0.3}_{-1.0}$	0.2–1.7 plus 2.45–3.0
C	0.9 ± 0.1	0.4–1.22 plus 1.7–2.12
	$0.0^{+1.5}_{-0.0}$	0.025–0.310 plus 0.43–0.585
Al	1.25 ± 0.2	1.20–2.1 plus 2.45–3.0
Si	1.15 ± 0.2	0.4–1.39 plus 1.6–2.21
	1.4 ± 0.3	0.27–1.79 plus 2.07–2.93

V. CONCLUSIONS

Energy straggling of protons has been measured by a backscattering technique for protons incident on Be, C, Al, and Si targets with energies in the range of 0.2–3.0 MeV. The backscattering technique involves monitoring the width of a sharp feature in the backscattered energy spectrum as a function of the amount of target material traversed by the protons. The problems with thin-film thickness nonuniformities are eliminated by the use of the technique. The technique is limited, however, to those target materials which have "resonances" or other sharp features in their scattering cross sections. Also, since the width of such features in the *observed* spectra is strongly affected by the energy dependence of the proton stopping power $S(E)$, uncertainties in $S(E)$ can also limit the accuracy of the resultant straggling parameters, particularly when broad resonances are involved. Finally, since the resultant values for the straggling parameters are averages over the energies experienced by the protons on the inbound and outbound trajectories in the target, an accurate and detailed energy dependence cannot be easily obtained by this method.

ACKNOWLEDGMENTS

We would like to thank J. McDonald who carried out the bulk of the measurements reported here, and aided in the data reduction. We also acknowledge the help of S. M. Meyers who participated in setting up one of the earlier experiments, and we are grateful for his comments on the manuscript during its final preparation. This work was supported by the U. S. Department of Energy, under Contract No. AT(29-1)789.

*Present address: Oak Ridge National Laboratory, Oak Ridge, Tenn. 37830.
[1]E. Bonderup and P. Hvelplund, Phys. Rev. A 4, 562 (1971).
[2]W. K. Chu, Phys. Rev. A 13, 2057 (1976).
[3]P. Sigmund, Phys. Rev. A 14, 996 (1976).
[4]B. Efken, D. Hahn, D. Hilscher, and G. Wustfeld, Nucl. Instrum. Methods 129, 219 (1975).
[5]F. Besenbacher, J. Heinemeier, P. Hvelplund, and H. Knudsen, Phys. Lett. A 61, 75 (1977).
[6]G. MacKenzie and B. H. Armitage, Nucl. Instrum. Methods 133, 489 (1976); B. H. Armitage, J. D. F. Ramsay, and F. P. Brady, *ibid.* 149, 329 (1978).
[7]See, for example, J. M. Harris, W. K. Chu, and M-A. Nicolet, Thin Solid Films 19, 259 (1973); J. M. Harris and M-A. Nicolet, Phys. Rev. B 11, 1013 (1975); G. E. Hoffman and D. Powers, Phys. Rev. A 13, 2042 (1976).
[8]A. B. Chilton, John N. Cooper, and J. C. Harris, Phys. Rev. 93, 413 (1954).
[9]D. Olmos, F. Aldape, J. Cavillo, A. Chi, S. Romero, and J. Rickards, *Ion Beam Surface Layer Analysis,* edited by O. Meyer, G. Linker, and F. Kappeler (Plenum, New York, 1975), Vol. I, p. 65.
[10]This energy "bunching" effect has previously been observed experimentally by D. A. Sykes and S. J. Harris, Nucl. Instrum. Methods 94, 39 (1971).
[11]N. Bohr, K. Dans. Vidensk. Selsk. Mat. Fys. Medd. 18, 8 (1948).
[12]A brief account of this work has previously been presented in R. A. Langley and D. K. Brice, Nucl. Instrum. Methods 149, 195 (1978); D. K. Brice and R. A. Langley, *ibid.* 149, 191 (1978).
[13]F. S. Mozer, Phys. Rev. 104, 1386 (1956).
[14]H. L. Jackson, A. I. Galonsky, F. J. Eppling, R. W. Hill, E. Goldberg, and J. R. Cameron, Phys. Rev. 89, 365 (1953).
[15]E. A. Milne, Phys. Rev. 93, 762 (1954).
[16]F. C. Shoemaker, J. E. Faulkner, G. M. B. Bouricus, S. G. Kaufman, and F. P. Mooring, Phys. Rev. 83, 1011 (1951).
[17]T. Awaya, J. Phys. Soc. Jpn. 20, 669 (1965).
[18]A. Tveter, Nucl. Phys. A 185, 433 (1972).
[19]J. Vorona, J. W. Olness, W. Haeberli, and H. W. Lewis, Phys. Rev. 116, 1562 (1959).
[20]W. B. Gauster and I. J. Fritz, J. Appl. Phys. 45, 3309 (1974).
[21]R. A. Langley and R. S. Blewer, Thin Solid Films 19, 187 (1973).
[22]J. B. Mitchell, S. Agami, and J. A. Davies, Radiat. Eff. 28, 133 (1976).
[23]R. A. Langley, Phys. Rev. A 4, 1868 (1971).
[24]S. T. Picraux, "Lattice Location of Impurities in Metals and Semiconductors," in *New Uses of Ion Accelerators,* edited by J. F. Ziegler (Plenum, New York, 1975), p. 238.
[25]C. Tschalär, Nucl. Instrum. Methods 61, 141 (1968).
[26]D. K. Brice, Thin Solid Films 19, 121 (1973); E. I. Siritonin, A. F. Tulinov, A. Fiderkevich, and K. S. Shyskin, Vestn. Mosk. Univ. Fiz. Astronomiya 12, 541 (1971); D. Powers and W. Whaling, Phys. Rev. 126, 61 (1962).
[27]G. Deconninck and Y. Fouilhe, *Ion Beam Surface Layer Analysis,* edited by O. Meyer, G. Linker, and F. Käppeler (Plenum, New York, 1976), p. 87.
[28]D. K. Brice, Radiat. Eff. 11, 227 (1971).
[29]D. K. Brice, Phys. Rev. A 6, 1791 (1972).
[30]J. F. Janni, Air Force Weapons Laboratory Technical Report, AFWL-TR-65-150, Kirtland Air Force Base, Albuquerque, New Mexico, September, 1966 (unpublished).
[31]C. B. Madsen and P. Venkatswarlu, Phys. Rev. 74, 1782 (1948); C. B. Madsen, K. Dans. Vidensk. Selsk. Mat. Fys. Medd. 27, 13 (1953).
[32]L. P. Nielsen, K. Dans. Vidensk. Selsk. Mat. Fys. Medd. 33, 6 (1961).
[33]A. A. Bednyakov, U. V. Bulgakov, V. S. Nikolaev, V. P. Sobakin, and V. L. Chernov, Phys. Lett. A 62, 183 (1977).
[34]J. Lindhard and M. Scharff, K. Dans. Vidensk. Mat. Fys. Medd. 27, 15 (1953).